

Burgers Shock Waves and Sound in a 2D Microfluidic Droplets Ensemble

Tsevi Beatus,¹ Tsvi Tlusty,² and Roy Bar-Ziv¹

¹*Department of Materials and Interfaces, The Weizmann Institute of Science, Rehovot, Israel*

²*Department of Physics of Complex Systems, The Weizmann Institute of Science, Rehovot, Israel*

(Received 6 April 2009; published 11 September 2009)

We investigate the collective motion of a two-dimensional disordered ensemble of droplets in a microfluidic channel far from equilibrium and at Reynolds number $\sim 10^{-4}$. The ensemble carries ultraslow shock waves and sound, propagating at $\sim 100 \mu\text{m s}^{-1}$ and superposed on diffusive droplets motion. These modes are induced by long-range hydrodynamic dipolar interactions between droplets, the result of the symmetry breaking flow. The modes obey the Burgers equation due to a local coupling between droplets velocity and number density. This stems from a singular effect of the channel sidewall boundaries upon summation of the hydrodynamic interaction in two dimensions.

DOI: 10.1103/PhysRevLett.103.114502

PACS numbers: 47.61.-k, 47.55.D-

Nonequilibrium, dissipative many-body systems with long-range interactions exhibit complex collective dynamics, for example, elastic turbulence [1], non-Brownian sedimentation [2], and dusty plasma crystals [3]. The general description of such systems remains an open theoretical challenge [4]. Also in this class are microfluidic droplet ensembles [5–10], which exhibit complex dynamics due to hydrodynamic interactions. Yet these ensembles operate in a linear, low Reynolds number flow regime ($\text{Re} \sim 10^{-4}$), and are hence accessible both experimentally and theoretically. The simplest microfluidic ensemble is the one-dimensional (1D) microfluidic crystal—an ordered array of droplets, which exhibits unique acoustic modes, akin to solid state phonons, as well as nonlinear instabilities and anomalies related to boundaries [8,9]. These modes arise from hydrodynamic dipolar interactions between droplets that are induced by the symmetry breaking flow field. Theoretically, the phonons are entirely tractable due to the 1D crystalline order and the small fluctuations of droplets motion. In contrast, the many-body problem is far more complex when dealing with the dynamics of a 2D disordered ensemble, in which individual droplets move erratically, with large amplitude fluctuations and dynamic clustering.

In this Letter, we investigate the collective modes of such 2D disordered microfluidic droplet ensembles. Analyzing the fluctuations of droplet number density along the flow, we observe new collective modes—ultraslow shock waves and sound propagating at $\sim 100 \mu\text{m s}^{-1}$, despite the heavy dissipation. These waves are superposed on the complex motion of individual droplets. Surprisingly, we find that the waves obey the 1D Burgers equation [11] as a direct result of a local linear coupling between droplet number density and their velocity. We show theoretically that this coupling arises from summation over the two-body dipolar interaction under a mean-field approximation. This is a singular consequence of the channel sidewall boundaries, which is a marginal case of the known divergence of long-range interactions in 3D [2,12]. The re-

nown Burgers equation was introduced in the 1930s as a simplified version of the Navier-Stokes equation [11] and has been used to study diverse nonequilibrium, nonlinear phenomena in turbulence [13], cosmology [14], and interface dynamics [15]. To the best of our knowledge, despite the extensive theoretical work on this equation, there is a lack of relevant experimental systems besides second sound in liquid helium [16,17] and dusty plasma [18]. The 2D disordered droplet ensemble is, therefore, a new tabletop experiment for studying Burgers dynamics.

To investigate the dynamics of a two-dimensional ensemble of droplets we built a microfluidic droplet generator [5,8,9]. Water droplets formed at a T junction between water and oil channels under continuous flow, emanating at a constant rate with uniform radii $R = 6\text{--}15 \mu\text{m}$ (Fig. 1). The T junction, $25 \mu\text{m}$ in width, was connected to a wider channel of width $W = 500 \mu\text{m}$ or $800 \mu\text{m}$, where the droplets formed a 2D disordered ensemble flowing at a mean velocity $u_d \simeq 100 \mu\text{m s}^{-1}$ (Fig. 1; movie 1 [19]). The channel height was $h = 10 \mu\text{m} < 2R$; hence, the droplets had a disklike shape, squeezed between the channel floor and ceiling. These boundaries imposed friction

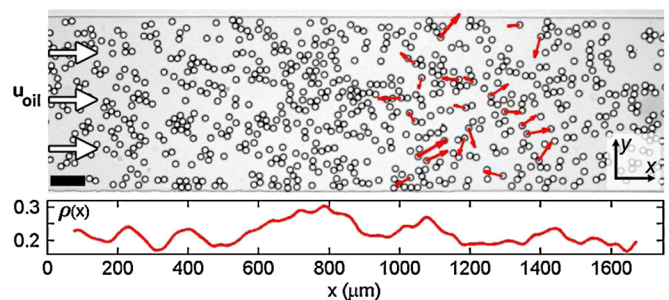


FIG. 1 (color online). Disordered 2D ensemble of microfluidic water-in-oil droplets. (top) Droplets flowing in a $500 \mu\text{m}$ width channel, $\rho_0 = 0.23$. Red vectors show droplet velocities relative to u_d . Distilled water and light mineral oil with 2% Span-80 surfactant (w/w) were used. Scale bar is $100 \mu\text{m}$. (bottom) The corresponding 1D density profile $\rho(x, t)$.

that slowed the droplets relative to the mean velocity of the dragging oil [8], $u_{\text{oil}}^{\infty} \approx 400 \mu\text{m s}^{-1}$. The Reynolds number of the system was estimated as $\text{Re} = u_{\text{oil}} \rho_{\text{oil}} h / \eta_{\text{oil}} \sim 10^{-4}$, where $\rho_{\text{oil}} = 800 \text{ kg/m}^3$ and $\eta_{\text{oil}} = 30 \text{ mPa s}$ are oil density and viscosity. The mean area fraction of the droplets, ρ_0 , was controlled by adjusting the gas pressure at the water and oil inlets, and varied between 0.06 and 0.60. Using a motorized microscope stage moving in frame at u_d , we followed up to 2000 droplets for $\sim 100 \text{ s}$ and extracted their trajectories (movie 2 [19]).

Droplets density was nonuniform on many length scales, and individual droplets exhibited random motion due to interparticle interactions and dynamic clustering [Fig. 2(a), Fig. s1 [19]] [20]. At short time scales, $t < 0.5 \text{ s}$, droplets

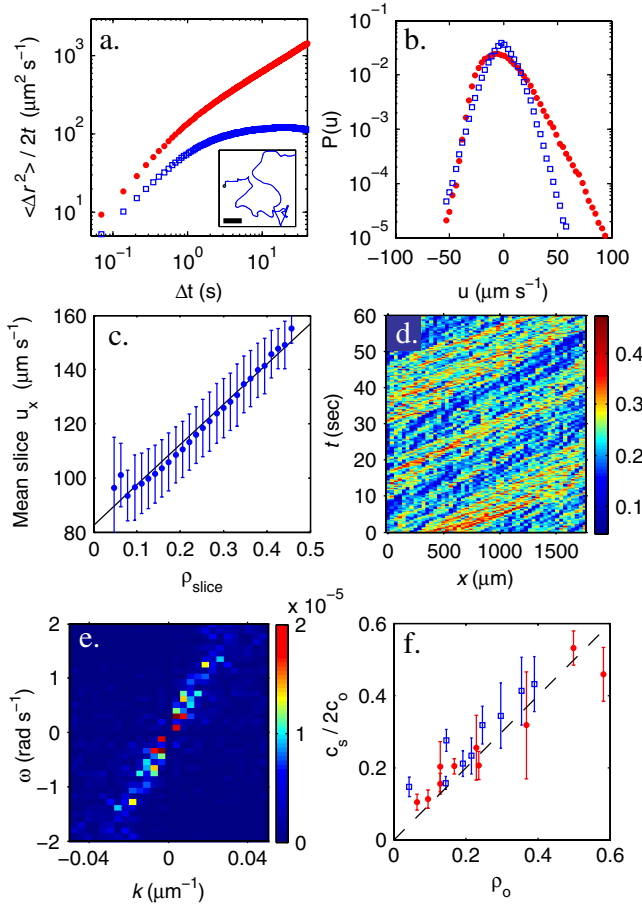


FIG. 2 (color online). (a) Mean square displacement over time along x (red circles) and y (blue squares) vs time for $\rho_0 = 0.10$. Zero slope corresponds to diffusion. Inset: a typical trajectory. Scale bar is $50 \mu\text{m}$. (b) Droplet velocity distributions: u_x (red circles) and u_y (blue squares). (c) Mean u_x in $2R$ slices vs slice density for $\rho_0 = 0.23$ (dots) with standard deviation bars and linear fit with slope $\alpha = 150 \mu\text{m s}^{-1}$ (solid line). (d) Space-time diagram of $\rho(x, t)$ for $\rho_0 = 0.23$. Color encodes for local density. (e) The power spectrum of $\rho(x, t)$ shown in (d) in units of $(\mu\text{m s})^{-2}$. (f) Normalized sound velocity vs mean density ρ_0 for $W = 500 \mu\text{m}$ (red circles) and $W = 800 \mu\text{m}$ (blue squares). A numerical simulation of the droplet ensemble (Fig. s5 [19]) gave similar results to (a–f).

motion was ballistic over distances of $\sim R$, and at longer time scales droplets exhibited diffusion and superdiffusion: Perpendicular to the flow, droplet trajectories were diffusive ($\Delta y^2 = D_y t$, $D_y \sim 300 \mu\text{m}^2 \text{ s}^{-1}$) with a symmetric velocity distribution, while along the flow their trajectories were superdiffusive ($\Delta x \propto t^\nu$, $\nu \approx 1.4$) with an asymmetric velocity distribution, reflecting the broken symmetry of the system [Figs. 2(a) and 2(b)].

To simplify these complex dynamics, we reduced the 2D density field to a 1D density profile $\rho(x, t)$ along the flow (Fig. 1). This was done by measuring the local area fraction in discrete narrow slices perpendicular to the flow with length Δx of a few droplet radii and width $\Delta y = W$. The mean velocity of droplets within a slice, $u(x, t)$, increased linearly with slice density [Fig. 2(c)]: $u(x, t) = u_0 + \alpha \rho(x, t)$, where $u_0 \sim 100 \mu\text{m s}^{-1}$ is the velocity of an isolated droplet and $\alpha \sim 100\text{--}150 \mu\text{m s}^{-1}$ is the coupling constant between local droplets velocity and their number density. In our experiments $\alpha \sim 1.7c_0$ for $\rho_0 < 0.3$, approaching $\alpha \sim c_0$ for $\rho_0 \sim 0.6$, where $c_0 = (u_d/u_{\text{oil}}^{\infty})(u_{\text{oil}}^{\infty} - u_d)$ is the natural velocity scale in the system [8]. The space-time diagram of $\rho(x, t)$ revealed large-scale fluctuations, hundreds of microns long, propagating along the flow, as measured in the frame of reference moving at u_d [Fig. 2(d)]. From the power spectrum of $\rho(x, t)$ we obtained a linear dispersion relation $\omega(k) = c_s k$ between frequency ω and wave vector k [Fig. 2(e)], with a sound velocity of $c_s = 10\text{--}100 \mu\text{m s}^{-1}$ and frequencies of less than 0.5 Hz . The sound velocity scales with density, $c_s \sim 2c_0 \rho_0$, and is independent of W [Fig. 2(f)].

To examine the dynamics of large density fluctuations we generated a short pulse of 200–300 droplets and followed their motion [Figs. 3(a) and 3(b), movies 3 and 4 [19]]. Markedly, the droplets self-organized into a shock wave structure with a discontinuous density jump at the front, and a rarefaction at the rear that increased with time. The front line was perpendicular to the flow and its density decreased in time. Propagating at $u_{\text{shock}} = 145 \mu\text{m s}^{-1}$, the shock wave kept its asymmetric shape although individual droplets changed their relative position within the pack and despite their diffusive motion. Traces of shock waves were found also in experiments with continuous droplet formation as dense, small-scale fronts $\sim 100 \mu\text{m}$ long in the x direction. The fronts formed spontaneously, propagating for $1\text{--}2 \text{ s}$ before spreading out [Figs. 3(c)–3(e)]. They were not a mere advection of matter, since they propagated into lower density regions by engulfing the droplets ahead. As shock waves, these fronts were “supersonic”: they propagated faster than the estimated speed of sound in the medium ahead: $u_{\text{front}} > 2c_0 \rho_R$, where ρ_R is the droplet density ahead of the front.

Theory.—Droplets conservation implies $\partial_t \rho + \partial_x(u\rho) = \mathbf{D}[\rho]$ with $u\rho$ the advective flux and \mathbf{D} a diffusion operator. Substituting the velocity-density coupling, neglecting small fluctuations $\delta u/u \sim 10\%$ [Fig. 2(c)], and transferring into a moving frame, $x' \equiv (x - u_0 t)/2\alpha$, we

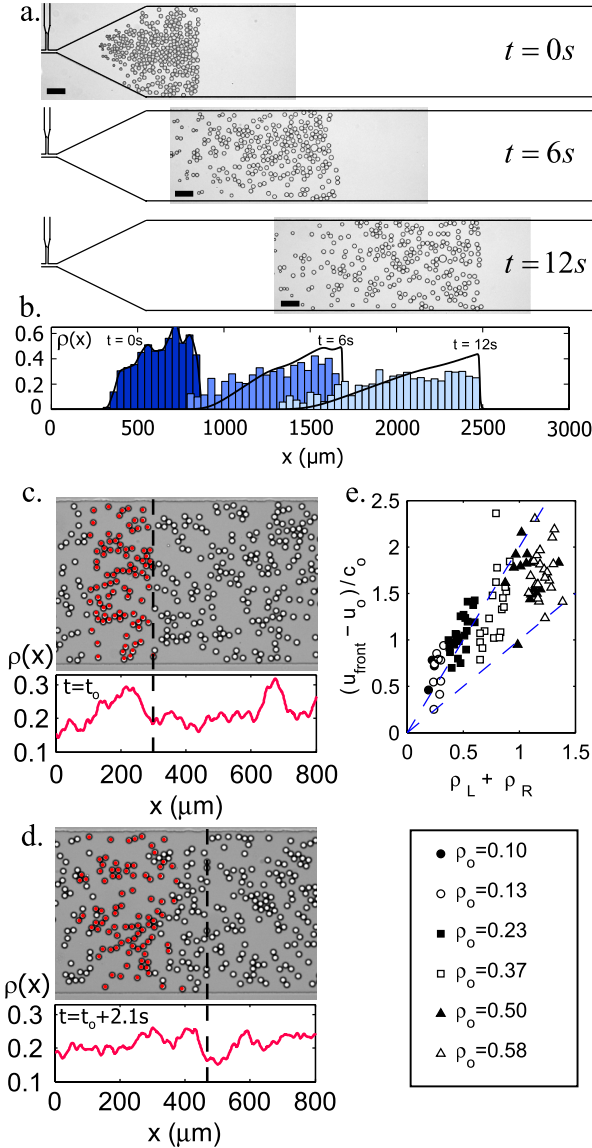


FIG. 3 (color online). Shock waves. (a) shock wave evolution in time shown at 6s intervals in the frame of the channel (solid lines) and (b) the corresponding density profiles $\rho(x, t)$ for each snapshot (bars). The black line shows the solution of the Burgers equation for the experimental initial condition with $c_0 = 150 \mu\text{m s}^{-1}$ and $u_0 = 100 \mu\text{m s}^{-1}$. Scale bars are $100 \mu\text{m}$. (c–d) A shocklike front in a continuous experiment and its $\rho(x, t)$. (c) The front is marked by a dashed line, and the droplets on its left side are gray (red). (d) After 2.1s the front line moved, engulfing new droplets. (e) Normalized front velocity for different ρ_0 vs the sum of the densities at the two sides of the front. Dashed lines have slope of 1 and 2.

obtain the 1D Burgers equation:

$$\partial_t \rho + \rho \partial_x \rho = \mathbf{D}[\rho]. \quad (1)$$

For superdiffusion, we use $\mathbf{D}[\rho] = (D_0/4a^2) \partial_{xx} \rho^{2/\nu+1}$ [21] with $D_0 \approx 75 \mu\text{m}^2 \text{s}^{-1}$ and $\nu = 1.4$ (for other formulations see [22,23]). However, droplet superdiffusion can be neglected compared to the advection term since

$D_0/[(2\alpha)^2 \Delta x'] \sim 0.01$. The solutions of the Burgers equation are shock waves with a sharp front and rarefaction at the rear [11,13] as seen experimentally (Fig. 3, Fig. s2 [19]). The velocity of a Burgers shock is obtained from mass conservation across its front and depends on the mean density at both its sides: $u_{\text{shock}} = u_0 + \alpha(\rho_L + \rho_R)$. The typical width of the front is $O(D_0/\alpha\Delta\rho) \sim 1 \mu\text{m}$, where $\Delta\rho$ is its amplitude [11]. Indeed, the shock in Fig. 3(a) had $u_0 \approx 100 \mu\text{m s}^{-1}$, $\alpha \approx 150 \mu\text{m s}^{-1}$, $\rho_L \approx 0.4\text{--}0.5$, and $\rho_R = 0$, which implies $u_{\text{shock}} = 160\text{--}175 \mu\text{m s}^{-1}$. The front width is narrow, which corroborates that diffusion is negligible. The shock is supersonic as it is faster than the speed of sound in the medium ahead, $c_s \approx u_0$. A numeric solution of the Burgers equation with the experimental parameters and initial condition is in good agreement with the measured density profile [Fig. 3(b) and movie 4 [19]]. Additionally, a numeric simulation of the 2D droplets ensemble shows similar dynamics (supplementary material and movies 5 and 6 [19]). The prediction for u_{shock} applies also for the velocity of the shocklike fronts [Fig. 3(e)]. Furthermore, their fast decay (1–2s) relative to the isolated shock [Fig. 3(a)] is consistent with the Burgers equation, in which narrow structures typically decay faster (Fig. s2 [19]). The Burgers equation also explains sound in the system, as infinitesimal shocks with $\rho_L \approx \rho_R \approx \rho_0$. Ignoring diffusion and expanding (1) to small density fluctuations $\rho(x, t) = \rho_0 + \delta\rho(x, t)$ with $\delta\rho \ll \rho_0$ yields a first-order wave equation: $(\partial_t + \alpha\rho_0\partial_x)\delta\rho = 0$ with traveling-wave solutions that propagate forward at $c_s = \alpha\rho_0$ in the frame moving at $u_d = u_0 + \alpha\rho_0$, as in the experiment [Fig. 2(f)].

Our Burgers theory is based only on droplet conservation and the measured linear velocity-density coupling. To explain the coupling α in terms of the hydrodynamic interactions between the droplets, we use a mean-field approximation to calculate the velocity change, Δu_x , of a test droplet due to its interactions with a uniformly distributed ensemble of droplets of area fraction ρ_0 .

In the low Reynolds regime, where inertia is negligible, droplet motion is governed by drag and friction forces only. The drag force is given by $F_{\text{drag}} = \xi_d[u_{\text{oil}}(\mathbf{r}) - u_d]$ with drag coefficient $\xi_d = 8\pi\eta R^2/h$ and $u_{\text{oil}}(\mathbf{r})$ the velocity of oil at the droplet's position, which includes perturbation of other droplets. Friction force stems from energy dissipation due to a treadmill flow inside the droplet and is proportional to its velocity $F_f = \mu u_d$ with friction coefficient $\mu \approx 0.03 \text{ g s}^{-1}$. Balancing drag and friction we obtain the equation of motion of the n th droplet: $\dot{\mathbf{r}}_n = (1 + \mu/\xi_d)^{-1} u_{\text{oil}}(\mathbf{r}_n)$, in which we can calibrate the constant $(1 + \mu/\xi_d)^{-1} = (u_0/u_{\text{oil}}^\infty)$ for an isolated droplet [8].

The motion of each droplet perturbs the flow of oil around it, which mediates a hydrodynamic interaction between the droplets. The flow is well approximated by a 2D potential flow with potential ϕ , such that $\nabla\phi$ is the velocity field induced by the droplet [8,24–26], and the drag force between two droplets is given by

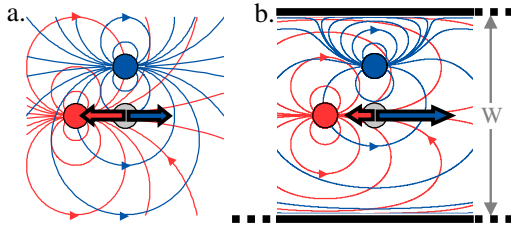


FIG. 4 (color online). The dipolar drag forces of two droplets acting on a test droplet (pale gray). Without sidewalls (a), longitudinal drag forces cancel out. Under confinement (b) droplet fields are screened, leading to a net drag force along x .

$F_{\text{drag}} = \xi_d \nabla \phi(\mathbf{r}_n, \mathbf{r}_i)$. Without sidewalls the potential is that of a 2D dipole, but when sidewalls are introduced, it is distorted and screened as $\exp(-2\pi x/W)$, with an explicit y dependence due to the breaking of translational invariance [9]. The confined flow potential is calculated using the method of electrostatic image charges by introducing an infinite array of image dipoles along y [9,27]. Hence, in the equation of motion of the n th droplet we have $u_{\text{oil}}(\mathbf{r}_n) = u_{\text{oil}}^{\infty} \hat{x} + \sum_{i \neq n} \nabla \phi(\mathbf{r}_n, \mathbf{r}_i)$.

Under the mean-field approximation we show that the source of the velocity-density coupling is the sidewall boundaries. If there were no sidewalls, we would obtain that the uniform droplets distribution, which spans the entire xy plane, induces $\Delta u_x = 0$ on the test droplet. This stems from the symmetry of the unconfined dipole and can be seen, for example, by dividing the droplets in the uniform distribution into pairs, whose velocity contributions to $u_{\text{oil}}(\mathbf{r}_n)$ cancel out [Fig. 4(a)]. Under confinement, however, each of these pairs induces a positive net contribution to $u_{\text{oil}}(\mathbf{r}_n)$ due to screening; hence $\Delta u_x > 0$ [Fig. 4(b)]. To calculate Δu_x , we integrate the velocity contributions of the droplets in a slab around the test droplet $\Delta u_x = (u_0/u_{\text{oil}}^{\infty}) \int \partial_x \phi(\mathbf{r}, \mathbf{r}') d^2 \mathbf{r}'$, which can be converted into a contour integral using the Stokes theorem $(u_0/u_{\text{oil}}^{\infty}) \oint \phi \hat{y} \cdot d\mathbf{l}$ (Fig. s3 [19]). To first order in $R/W \ll 1$ we obtain a linear coupling between velocity and density with $\alpha = c_0$, identical to the experiment within a factor of 1 to 2 [Figs. 2(f) and 3(e)]. This result is independent of the test droplet's y coordinate as well as the slab length, and hence applies locally and depends only on the density in a $4R$ slab around the droplet. The coupling is independent of W , which is peculiar since in the absence of sidewalls $\Delta u_x = 0$. The velocity-density coupling is, therefore, a singular consequence of the confining boundaries; namely, it vanishes without boundaries but is independent of their separation.

The 1D description captures the collective modes of the system—density and shock waves—although it ignores many degrees of freedom that arise from its 2D, discrete nature, such as transversal velocity [Figs. 1 and 2(b)]. These “hidden variables” are reflected, for example, in the measured variance of the linear velocity-density coupling [Fig. 2(c)]. We verified that nonuniformities perpen-

dicular to the flow do not waive the effective description by the 1D Burgers equation (Fig. s4 [19]). Finally we performed a numerical simulation of the 2D experiment, solving the equations of motion of up to 1000 droplets with periodic boundary conditions along x , which reproduced the experimental dynamics (Fig. s5 [19]). Operating in a linear flow regime, microfluidic droplet ensembles are a tabletop experiment that opens a vista into the nonequilibrium physics of many-body systems with long-range interactions, as well as Burgers dynamics and turbulence.

We wish to thank Assaf Avidan, Etam Benger, Haim Diamant, Gregory Falkovich, Elisha Moses, and Victor Steinberg.

-
- [1] A. Groisman and V. Steinberg, *Nature (London)* **405**, 53 (2000).
 - [2] S. Ramaswamy, *Adv. Phys.* **50**, 297 (2001).
 - [3] G. E. Morfill *et al.*, *Appl. Phys. B* **89**, 527 (2007).
 - [4] D. Ruelle, *J. Stat. Phys.* **95**, 393 (1999).
 - [5] T. Thorsen, R. W. Roberts, F. H. Arnold, and S. R. Quake, *Phys. Rev. Lett.* **86**, 4163 (2001).
 - [6] D. R. Link, S. L. Anna, D. A. Weitz, and H. A. Stone, *Phys. Rev. Lett.* **92**, 054503 (2004).
 - [7] P. Garstecki, M. J. Fuerstman, and G. M. Whitesides, *Nature Phys.* **1**, 168 (2005).
 - [8] T. Beatus, T. Tlusty, and R. Bar-Ziv, *Nature Phys.* **2**, 743 (2006).
 - [9] T. Beatus, R. Bar-Ziv, and T. Tlusty, *Phys. Rev. Lett.* **99**, 124502 (2007).
 - [10] M. Baron, J. Bławdziewicz, and E. Wajnryb, *Phys. Rev. Lett.* **100**, 174502 (2008).
 - [11] J. M. Burgers, *The Nonlinear Diffusion Equation* (D. Reidel Publishing Company, Dordrecht-Boston, 1974).
 - [12] R. E. Caflisch and J. H. C. Luke, *Phys. Fluids* **28**, 759 (1985).
 - [13] J. Bec and K. Khanin, *Phys. Rep.* **447**, 1 (2007).
 - [14] Y. B. Zel'Dovich, *Astron. Astrophys.* **5**, 84 (1970).
 - [15] M. Kardar, G. Parisi, and Y. C. Zhang, *Phys. Rev. Lett.* **56**, 889 (1986).
 - [16] S. Kitabatake and Y. Sawada, *J. Phys. Soc. Jpn.* **45**, 345 (1978).
 - [17] L. S. Goldner, N. Mulders, and G. Ahlers, *J. Low Temp. Phys.* **93**, 131 (1993).
 - [18] S. Ghosh *et al.*, *Phys. Plasmas* **10**, 977 (2003).
 - [19] See EPAPS Document No. E-PRLTAO-103-013939 for supplementary movies. For more information on EPAPS, see <http://www.aip.org/pubservs/epaps.html>.
 - [20] F. Rouyer, D. Lhuillier, J. Martin, and D. Salin, *Phys. Fluids* **12**, 958 (2000).
 - [21] H. Spohn, *J. Phys. I (France)* **3**, 69 (1993).
 - [22] B. O'Shaughnessy and I. Procaccia, *Phys. Rev. Lett.* **54**, 455 (1985).
 - [23] R. Metzler and J. Klafter, *Phys. Rep.* **339**, 1 (2000).
 - [24] N. Liron and S. Mochon, *J. Eng. Math.* **10**, 287 (1976).
 - [25] T. Tlusty, *Macromolecules* **39**, 3927 (2006).
 - [26] H. Diamant, *J. Phys. Soc. Jpn.* **78**, 041002 (2009).
 - [27] J. Bławdziewicz and E. Wajnryb, *Phys. Fluids* **20**, 093303 (2008).